

Article

First Experience with Sentinel-2 Data for Crop and Tree Species Classifications in Central Europe

Markus Immitzer ^{*,†}, Francesco Vuolo [†] and Clement Atzberger

Institute of Surveying, Remote Sensing and Land Information (IVFL), University of Natural Resources and Life Sciences, Vienna (BOKU), Peter Jordan Strasse 82, 1190 Vienna, Austria; francesco.vuolo@boku.ac.at (F.V.); clement.atzberger@boku.ac.at (C.A.)

* Correspondence: markus.immitzer@boku.ac.at; Tel.: +43-01-47654-85732

† These authors contributed equally to this work.

Academic Editors: Parth Sarathi Roy and Prasad S. Thenkabail

Received: 14 January 2016; Accepted: 15 February 2016; Published: 23 February 2016

Abstract: The study presents the preliminary results of two classification exercises assessing the capabilities of pre-operational (August 2015) Sentinel-2 (S2) data for mapping crop types and tree species. In the first case study, an S2 image was used to map six summer crop species in Lower Austria as well as winter crops/bare soil. Crop type maps are needed to account for crop-specific water use and for agricultural statistics. Crop type information is also useful to parametrize crop growth models for yield estimation, as well as for the retrieval of vegetation biophysical variables using radiative transfer models. The second case study aimed to map seven different deciduous and coniferous tree species in Germany. Detailed information about tree species distribution is important for forest management and to assess potential impacts of climate change. In our S2 data assessment, crop and tree species maps were produced at 10 m spatial resolution by combining the ten S2 spectral channels with 10 and 20 m pixel size. A supervised Random Forest classifier (RF) was deployed and trained with appropriate ground truth. In both case studies, S2 data confirmed its expected capabilities to produce reliable land cover maps. Cross-validated overall accuracies ranged between 65% (tree species) and 76% (crop types). The study confirmed the high value of the red-edge and shortwave infrared (SWIR) bands for vegetation mapping. Also, the blue band was important in both study sites. The S2-bands in the near infrared were amongst the least important channels. The object based image analysis (OBIA) and the classical pixel-based classification achieved comparable results, mainly for the cropland. As only single date acquisitions were available for this study, the full potential of S2 data could not be assessed. In the future, the two twin S2 satellites will offer global coverage every five days and therefore permit to concurrently exploit unprecedented spectral and temporal information with high spatial resolution.

Keywords: Sentinel-2; forest; cropland; classification; Random Forest

1. Introduction

The Sentinel-2A satellite was successfully launched on 23 June 2015, as part of the European Copernicus program and the first scenes were delivered a few days later [1]. Sentinel-2 (S2) carries an innovative wide-swath, high-resolution, multispectral imager (MSI) with 13 spectral bands; this is going to offer unprecedented perspectives on our land and vegetation [2,3]. The combination of high resolution (up to 10 m), novel spectral capabilities (e.g., three bands in the red-edge plus two bands in the SWIR), wide coverage (swath width of 290 km) and minimum five-day global revisit time (with twin satellites in orbit) is expected to provide extremely useful information for a wide range of land (and coastal) applications [4].

In preparation for this new satellite mission, the scientific community has been working to provide feedback to system developers to define the best algorithms and data exploitation strategies. This activity resulted in several experiments based on simulated S2 datasets [5–15]. These studies reported a high potential of S2 in various fields of application. This potential in Earth Observation (EO), however, needs to be confirmed by real data.

Actual S2 data are now available and ready for exploitation for scientific and commercial purposes. With the present study, a first assessment of the S2 land cover mapping capabilities is undertaken by using pre-operational (August 2015) S2 images acquired over two test sites located in Central Europe. The preliminary assessment focuses on crop type and tree species mapping. Both are important for remote sensing applications.

Crop type maps produced before the end of the season, for example, are requested by policy- and decision-makers for management, statistics and economic purposes, as well as by Earth system scientists as input in crop models. Inglada *et al.* [16] recently revised the state-of-the-art in crop mapping using simulated S2 data. The study indicates that crop type maps, detailed enough to monitor individual parcels, are not globally available and that the data stream from S2 will offer a high potential to fill the gap between the availability of timely and accurate crop type maps and the user's needs. The study also performed a benchmarking of different classification algorithms highlighting the adequacy of the Random Forest (RF) classifier for land cover mapping. Scientific efforts are ongoing to integrate these algorithms in operative tools to use with S2 data, for instance within the S2 for Agriculture project funded by the European Space Agency (ESA), or the CropMon project funded by the Austrian Space Application Programme (ASAP). Within this context, our study contributes to the current state-of-the-art by reporting for the first time the application of the RF classifier to map crop types using actual S2 data.

Similarly, the classification approach was applied to a forest test site using one of the first available cloud-free S2 acquisition of Central Europe. Mapping tree species provides detailed description of forest ecosystems. This is necessary for ecological issues and sustainable forest management. Therefore, a large variety of sensors with a wide range of spatial and spectral resolution have been used in the past [17–19]. Besides providing descriptions of the actual forest composition, high repetition rates of satellite sensors facilitate the detection of changes caused by human as well as abiotic and biotic disturbances [20,21]. Both the actual mixture of species and the detection of changes and disturbances are information of increasing importance due to changing climate conditions [22].

The main objective of the study was to assess the suitability of S2 data for typical land cover classifications in agriculture and forestry using a supervised Random Forest (RF) classifier. As part of the case studies, we were also interested to see:

- i) how well object-based classifiers compare against a pixel-based approaches, and
- ii) which S2 spectral bands contribute most to the classification accuracy.

As the satellite has not yet reached its full operational mode/capacity, we were not yet able to exploit the temporal information. The study is preliminary as the analyzed images were only pre-operational. Some images still show some artifacts as demonstrated in Appendix A (Figures A1–3). All images analyzed in this study were released by ESA for first assessments and feedback.

2. Materials and Methods

2.1. Overview

To assess the potential of Sentinel-2 (S2) data for crop type and tree species mapping, we performed supervised classifications using the Random Forest (RF) classifier. Only pre-operational, single-date S2 images were used. The images were acquired in August 2015.

The workflow applied in this study is shown in Figure 1 and involved pixel- and object-based classifications for each case study (cropland and forest).

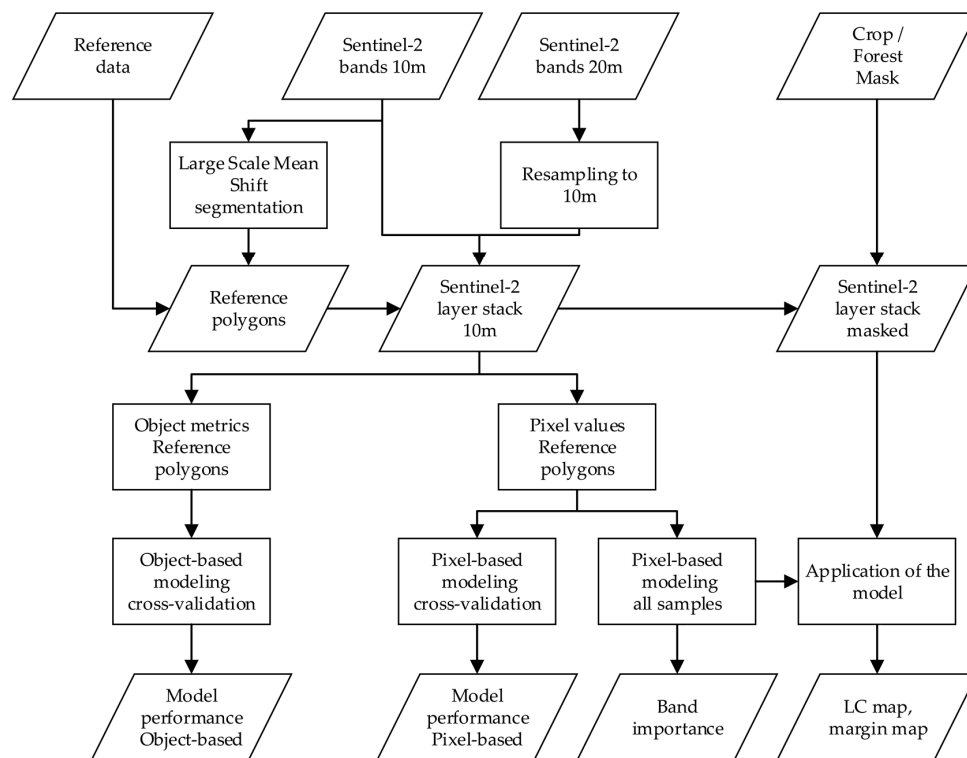


Figure 1. Workflow of the pixel- and object-based classification and validation.

The data preparation involved the resampling of the S2 bands acquired at 20 m to obtain a layer stack of 10 spectral bands at 10 m. An automatic Large Scale Mean Shift (LSMS) image segmentation was applied to the four S2 bands at 10 m pixel size (e.g., bands 2, 3, 4 and 8). The resulting objects were labeled using the reference data and exploited for training and validation. For the object-based classification, we used various band-specific metrics (Mean, Standard deviation, Min, Median, Max, 25th and 75th Percentile) extracted from the image objects. This led to 70 features for classification (10 bands \times 7 metrics). For the pixel-based classification, we used the reflectance in the ten spectral bands for each pixel.

Reference data for the supervised classification were acquired in two ways:

- during a field survey for the cropland test site, and
- from inventory data and visual interpretation of high spatial resolution images for the forest test site.

To cope with the limited number of reference samples, a 10-fold cross-validation approach [23] was chosen. Open Street Map (OSM) layers and CORINE Land Cover 2000 (CLC) [24] were used to mask out non-agricultural land for the crop study. The German ATKIS [25] dataset was used to mask out non-forest land for the forest study.

2.2. Sentinel-2 Data Sets

S2 carries an innovative wide-swath, high-resolution, multispectral imager (MSI) with 13 spectral bands with 10 to 60 m spatial resolution [3] (Figure 2). The first S2 image was acquired and processed on 27 June, only four days after launch [3,26]. For the present study, cloud-free Level 1C S2 images (ToA reflectance) acquired on 13 August (forest) and 30 August, 2015 (cropland), were used.

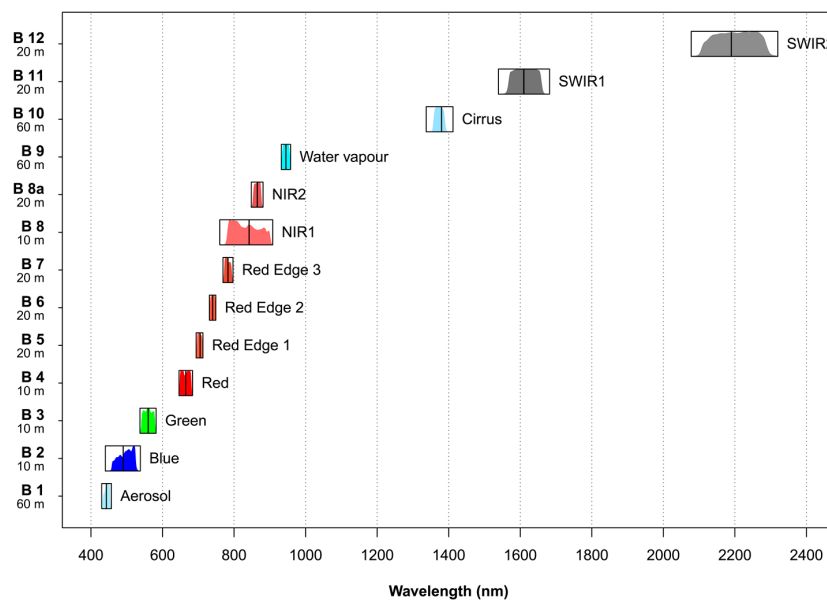


Figure 2. Characteristics of the Multi Spectral Instrument (MSI) on board Sentinel-2. The spectral response functions are shown in colors with the central wavelength in black. The band names and the corresponding spatial resolutions (in meters) are also indicated. For this study, the three “atmospheric” bands (e.g., B1, B9 and B10) were not used. Example images of all bands are shown in Appendix A.

The location of the test sites is shown in Figure 3, and detailed views in CIR composition of the S2 tile 33UXP for the crop classification and S2 tile 33 UXP for the tree species classification can be found in the following chapters.

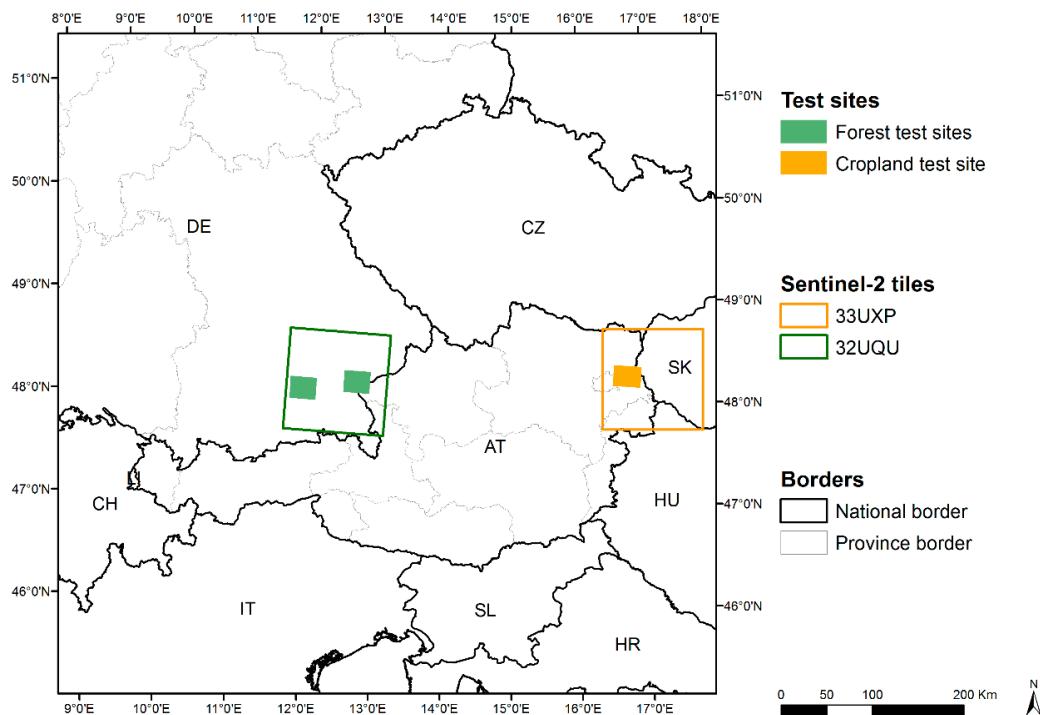


Figure 3. Location of cropland and forest test sites in Austria and Germany. Each site covers an area of about $10 \times 10 \text{ km}^2$. The extent of the respective S2 tiles is also indicated together with ESA’s scene naming convention.

The data was downloaded on 15 September, 2015. No radiometric or geometric pre-processing was applied. The S2 images were visually checked against existing raster data (SPOT-5, DEIMOS-1, Landsat-8, WorldView-2, and orthophotos) and showed a very good agreement, both in spatial and spectral terms. We visually compared the S2 images to orthophotos with 20 cm resolution and found a very good geometric accuracy. The generally high data quality of the analyzed images was further confirmed by the three atmospheric bands (Appendix A). It has to be noted, however, that some cirrus clouds, condensation trails and artifacts are visible in the cropland scene (Figure A1e).

2.3. Test Site 1: Marchfeld Cropland

The cropland site *Marchfeld* is located in the ~1000 km² Marchfeld region in Lower Austria (Lat. 48.20°N, Long. 16.72°E). In this area, cropland occupies about 60,000 ha, of which 21,000 ha are regularly irrigated. The location of the test site is shown in Figure 3—the corresponding S2 image is shown in Figure 4. Additional false color composites and images produced by Principal Component Analysis (PCA) can be found in Figure A1.

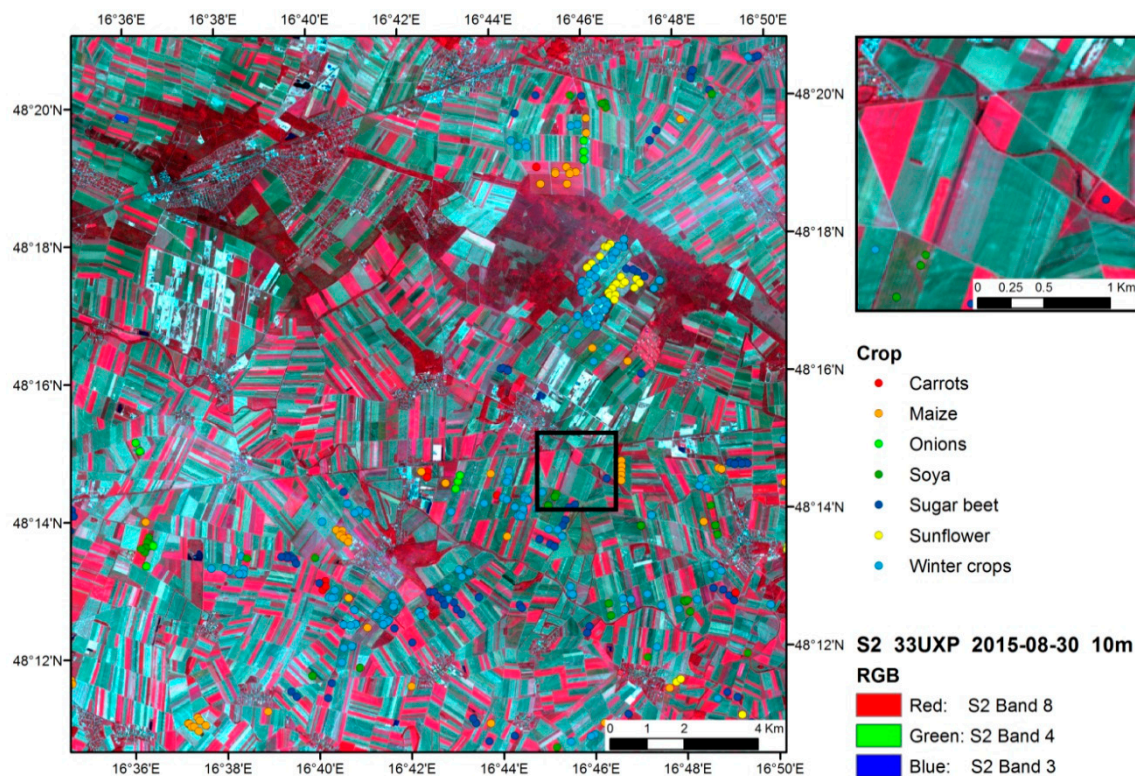


Figure 4. Sentinel-2 scene (30 August 2015) of the cropland test site *Marchfeld* in Lower Austria, Austria. The dots represent the centroids of the reference polygons used for classification. The top-right map shows the inter- and intra-field heterogeneity observed at the S2 spatial resolution of 10 m.

The Marchfeld region is characterized by a semi-arid climate with an average annual precipitation of 500–550 mm, and 200–440 mm between April–September. Annual precipitation can drop to 300 mm, making it the driest region of Austria. For example, in 2015, *Statistik Austria* estimated a loss of about one-fifth of the harvested vegetables (especially onions and carrots) compared to the previous year due to the long period of heat and drought.

The soil conditions in *Marchfeld* are characterized by a high spatial variability, including soils with low to moderate water-storage capacity [27–29]. The main crops cultivated during summer months are vegetables (11% of the crop area), sugar beet (10%) and potatoes (7%). Winter cereals are cultivated on about two-thirds of the crop area [30].

For the collection of the reference data, a field survey was carried out during the second half of August 2015. Crops were visually identified in the field. Coordinates were recorded using a GPS device. Agricultural fields with no crops were assigned to the class *winter crops* (harvested in June) by inspecting the crop residuals in field. A summary of the reference data is presented in Table 1. The different numbers of reference polygons reflect the prevailing cropping conditions in the study area. Average spectral signatures for the seven crop classes are shown in Figure 5.

Table 1. Reference samples from August 2015 for the cropland test site *Marchfeld*.

Crop type	Number of polygons	Average polygon size (in pixel)	Number of pixels
Carrots	32	290	9279
Maize	73	546	39,834
Onions	15	311	4672
Soya	53	383	20,299
Sugar beet	86	382	32,824
Sunflower	32	314	10,045
Winter crops ¹	161	703	113,222

¹ Note that winter crops had been harvested at the time of image acquisition (30 August, 2015). This class therefore represents bare soils.

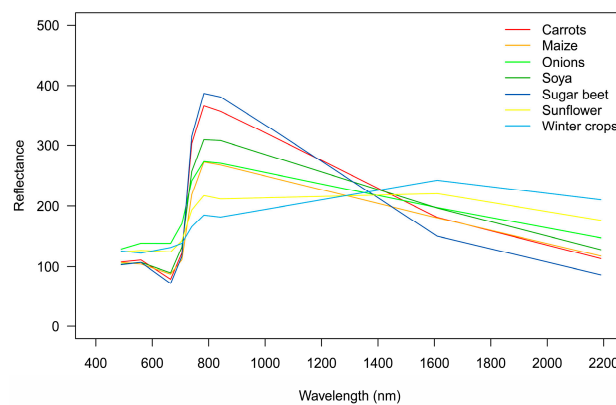


Figure 5. Average spectral signatures of the seven crop classes of cropland test site *Marchfeld*. The Top-of-Atmosphere (ToA) reflectance values (y-axis) are multiplied by a factor of 1000.

2.4. Test Site 2: Ebersberg and Altoetting Forests

The two forest sites *Ebersberg* and *Altoetting* are located east of Munich in Bavaria, Germany (Figure 3). The forests are mainly managed by the Bavarian State forest agency (BaySF). The mean annual temperature is around 7.6 °C; the average annual precipitation is 850–950 mm with around 500 mm between April–September. The soil conditions are mainly mesic-moist [31].

The natural forest vegetation of the region is a beech-dominated forest with different amount of spruce and fir. Forests are dominated today by Norway spruce (*Picea abies*, (L) Karst.). With amounts of around 10%, European beech (*Fagus sylvatica*, L.) and Scots pine (*Pinus sylvestris*, L.) play also an important role, followed by oak-species (*Oak sp.*) with coverage of around 5%. Further, (minor) tree species are Silver fir (*Abies alba*, Mill.), European larch (*Larix decidua*, Mill.), Douglas fir (*Pseudotsuga menziesii*, (Mirb.) Franco), European hornbeam (*Carpinus betulus*, L.), maple- (*Acer sp.*), birch- (*Betula sp.*), alder- (*Alnus sp.*), and willow-species (*Salix sp.*) [31].

Our analysis focused on the two largest connected forest areas: *Altoetting* and *Ebersberg*. These two forests are characterized by heterogeneous mixed forests with only few pure stands. The reference data (Figure 6) were obtained from forest inventory points acquired by the BaySF and visual interpretation of very high resolution image data (WorldView-2 and orthophotos).

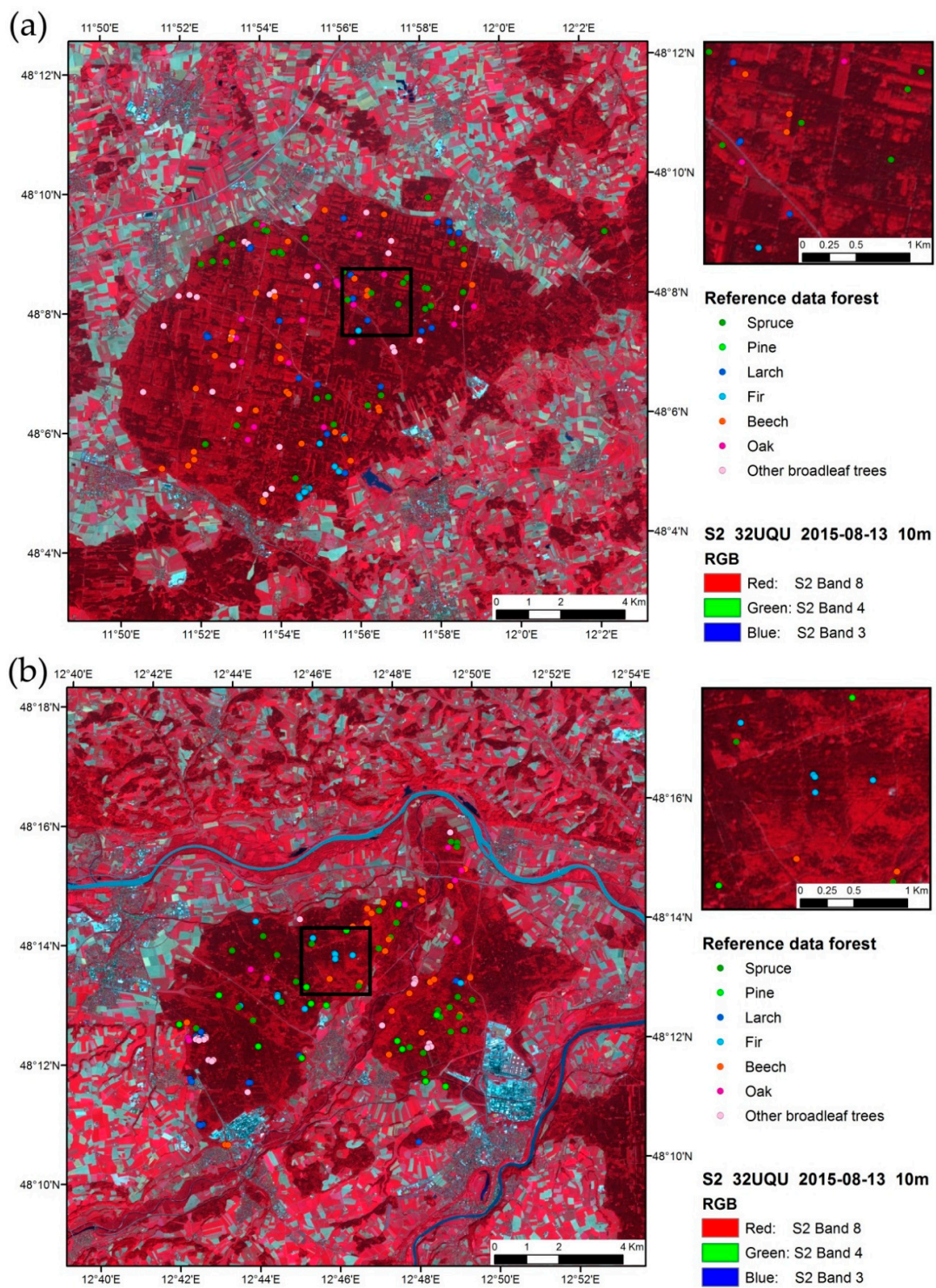


Figure 6. Sentinel-2 scene (13 August 2015) of the two forest test sites (a) *Ebersberg* and (b) *Altoetting* in Bavaria, Germany. The dots represent the centroids of the reference polygons used for classification. The top-right map shows forest heterogeneity observed at the S2 spatial resolution of 10 m.

The reference data (Table 2) from the two forest test sites were combined in one dataset and jointly used for analysis. As only few reference points were available for Douglas fir, we excluded this species from the analysis. The maple-, birch-, alder and willow-species were analyzed together with European hornbeam in the class “other broadleaf trees”.

Average spectral signatures of the seven analyzed tree species classes are shown in Figure 7. Note that the high reflectance value of band 2 (Blue) is due to the use of non-atmospherically corrected (ToA reflectance) data. Additional examples of false color composites and images produced by PCA are shown in Appendix A (Figures A2 and A2).

Table 2. Reference samples for test sites *Ebersberg* and *Altoetting*. Note the differences in the average polygon size resulting from different species composition (not all tree species form pure stands)

Dominate Tree Species	Number of Polygons	Average Polygon Size (in pixel)	Number of Pixels
Spruce (<i>Picea</i> sp.)	77	1151	88,607
Pine (<i>Pinus</i> sp.)	21	1622	34,062
Larch (<i>Larix</i> sp.)	38	45	1700
Fir (<i>Abies</i> sp.)	26	29	760
Beech (<i>Fagus</i> sp.)	66	106	6977
Oak (<i>Quercus</i> sp.)	32	275	8796
Other broadleaf trees ¹	57	206	11,764

¹ Includes mainly following species: European hornbeam, maple-, birch-, alder and willow-species.

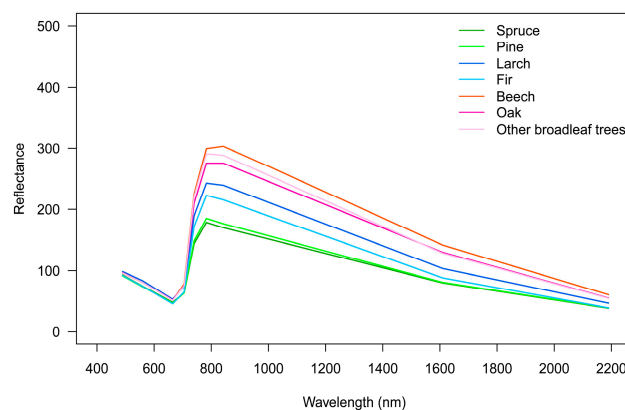


Figure 7. Average spectral signatures of the seven tree species of the forest test sites *Ebersberg* and *Altoetting*. The Top-of-Atmosphere (ToA) reflectance values (y-axis) are multiplied by a factor of 1000.

2.5. Segmentation

Besides a classical pixel-based mapping, we also aimed to assess the potential of S2 for object-based classifications. For this purpose, a Large Scale Mean Shift (LSMS) segmentation was applied using the four S2 bands recorded at 10 m (band 2, 3, 4 and 8). To reduce the effect of potential outliers on the segmentation, the data distributions in each layer were cut-off outside the 1st and 99th percentiles, respectively. Subsequently, pixel values in each layer were linearly stretched to range from 0 to 255 to give each layer the same importance. The mean shift algorithm is a non-parametric, feature-space analysis technique for locating the maxima of a density function developed by Fukunaga and Hostetler [32]. The algorithm does not require *a priori* knowledge about the shape or desired number of clusters and therefore is well suited for image segmentation. The algorithm extension to the spatial domain was proposed by Comaniciu and Meer [33].

In this study, we used the LSMS segmentation implemented in the open source software Orfeo Toolbox version 5.0.0. More information about LSMS can be found in Comaniciu and Meer [33] or in Ming *et al.* [34]. A detailed description of the Orfeo Toolbox is provided by Michel *et al.* [35]. The LSMS segmentation algorithm requires three parameters:

- Spatial Radius h_s (spatial distance between classes)
- Range Radius h_r (spectral difference between classes)

- Minimum size ms (merging criterion)

Several parameter sets were tested based on our experience and the results of the segmentation were visually evaluated using a *trial-and-error* approach. The final parameter sets for the two test sites are shown in Table 3. Due to the fragmentation and higher heterogeneity of the forest test sites, smaller segments were needed compared to the cropland segmentation. To achieve this, smaller range radius (hr) and smaller minimum size (ms) were used for the segmentation of the forest test sites.

Table 3. Parameter sets for the LSMS segmentation of the two test sites. For segmentation, only the four spectral bands at 10 m spatial resolution were used (e.g., bands 2, 3, 4 and 8).

Test Site	Spatial Radius (hs)	Range Radius (hr)	Minimum Size (ms)
Cropland (<i>Marchfeld</i>)	10	30	10
Forest (<i>Ebersberg & Altoetting</i>)	10	10	4

2.6. Random Forest (RF) Classification

The classifications were performed using the Random Forest (RF) classifier [36]. RF is a widely used machine learning algorithm consisting of an ensemble of decision trees. It uses bootstrap aggregating, *i.e.*, bagging, to create different training subsets to produce a diversity of trees, each providing a classification result for the samples not chosen. The output class is obtained as the majority vote of the outputs of a large number individual trees [36,37]. The algorithm produces an internal unbiased estimate of the generalization error, using the so-called “out-of-bag” (OOB) samples (which are not included in the training subset). In addition, RF provides a measure of the input features importance, called Mean Decrease in Accuracy (MDA), through random permutation, which can be used for feature ranking or selection [17,38–40]. The randomized sampling leads to increased stability and better classification accuracy compared to a single decision tree approach. RF is also relatively insensitive to the number of input data and multicollinearity of the data [41]. RF has been successfully applied in several regression and classification problems of EO data and generally achieves good results [17,38,40,42–48].

In this study we used the RF implementation *randomforest* [37] in R 3.2.3 [49]. A RF model requires the setting of two parameters:

- the number of trees to be grown in the run ($ntree$), and
- the number of features used in each split ($mtry$).

Several studies demonstrated that default model parameters often provide satisfactory results [17,37,50]. Therefore, we used the defaults values [36,37] and set $ntree$ to 500 trees, while $mtry$ was set equal to the square root of the total number of input features.

2.7. Accuracy Assessment

For validation of the RF-classification results, we used a 10-fold cross-validation approach [23]. This involved splitting the reference objects randomly in 10 sub-data sets, each including around 10% of the samples of each class. In each training step, a RF model was trained with 90% of the reference data and applied to the remaining 10% (*i.e.*, the validation data set). This step was repeated ten times. At the end, the ten results were aggregated to one confusion matrix. To permit a comparison between pixel- and object-based classification approaches, we split the pixels for the pixel-based classification using exactly the same partitions as applied to the object-based approach. Note that the splitting in 10 sub-data sets was not used for final map production. Instead, we used all reference samples to create new models, which were applied to the entire S2-scenes.

For pixel- and object-based classifications, the classification performance was assessed based on common statistical measures [51] derived from the confusion matrix. The selected statistical measures

included the overall accuracy (OA), the producer's accuracy (PA), the user's accuracy (UA) and the Kappa statistic.

To provide a measure of classification confidence, a *margin* value was calculated. This involved calculating the confidence *score*, being as the ratio of votes of the winning class to the total number of trees used in the classification. Higher scores indicate that the classifier is more confident in assigning a class. In the second step the *margin* was calculated as the proportion of votes for the winning class (*score*) minus the proportion of votes of the second class. The *margin* values were calculated for the pixel-based classifications providing additional information about the map reliability [45,52].

3. Results and Discussion

3.1. Crop Classification

The object-based classification for the cropland test site achieved a satisfactory (cross-validated) overall accuracy of 76.8% (Table 4). All classes reveal a well-balanced user's accuracy, while the producer's accuracy shows larger differences. The most accurately classified crops were sugar beet, maize and winter crops with producer's accuracies higher than 80%, followed by onions and soya. The three best-classified crops are the ones with the largest number of training samples (Table 1). They also reveal relatively high classification margins (Figure 8).

Table 4. Confusion matrix and statistical measures for the object-based crop classification for the cropland test site *Marchfeld*. Results were obtained using 10-fold cross-validation.

OBJECT-BASED	Carrots	Maize	Onions	Soya	Sugar Beet	Sun-Flower	Winter Crops	UA
Carrots	11	1	0	3	2	0	0	0.647
Maize	8	58	1	9	9	5	3	0.624
Onions	0	1	11	0	2	0	0	0.786
Soya	3	4	2	33	3	0	0	0.733
Sugar beet	10	6	1	5	70	1	0	0.753
Sunflower	0	1	0	1	0	9	3	0.643
Winter crops	0	2	0	2	0	17	155	0.881
PA	0.344	0.795	0.733	0.623	0.814	0.281	0.963	
							OA	0.768
							Kappa	0.699

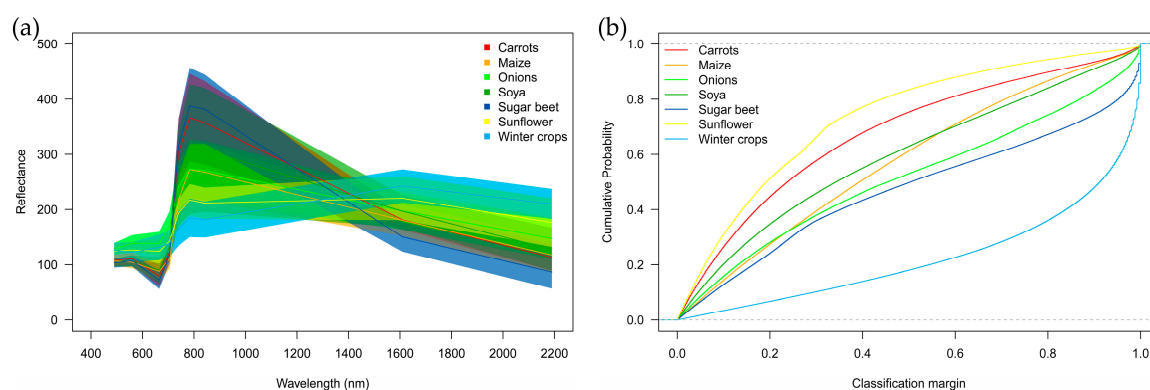


Figure 8. Spectral signatures and classification margins of the cropland test site *Marchfeld*. (a) Spectral signatures of the seven crop classes including the specific intra-class standard deviations. The Top-of-Atmosphere (ToA) reflectance values (y-axis) are multiplied by a factor of 1000. (b) Classification *margins* of the seven crop classes displayed as cumulative frequency distributions.

The two most problematic classes were carrots and sunflower achieving only producer's accuracies of around 30%. For carrots, the most common confusion was with sugar beet and maize.

Sunflower was often confused with winter crops, most probably due to the fact that sunflower was already in the senescence phase at the time of the Sentinel-2 image acquisition. This led to a large overlap with the spectral signature of bare soils (e.g., winter crops) and generally low classification margins (Figure 8).

Compared to the object-based approach (Table 4), slightly better classification results were obtained using the pixel-based classification (Table 5) with cross-validated OA = 83.2% vs. 76.8%. However, compared to the object-based approach, larger variations in the user's accuracy were found. The difficulty to correctly classify carrots and sunflower remained, with sunflower achieving slightly improved results (44% instead of 28%). The pixel-based classification also revealed an additional confusion between sunflower and onions and, in the case of onions, confusion with winter crops and sunflower. Due to its canopy structure, onions present a high proportion of visible soil and this might have caused confusion with bare soil pixels (winter crops) and sunflower.

Table 5. Confusion matrix and statistical measures for the pixel-based crop classification for the cropland test site *Marchfeld*. Results were obtained using 10-fold cross-validation.

PIXEL-BASED	Carrots	Maize	Onions	Soya	Sugar Beet	Sun-flower	Winter Crops	UA
Carrots	3130	248	40	1019	1225	23	140	0.537
Maize	1133	32,246	89	3446	2676	426	1467	0.777
Onions	48	42	3193	29	186	475	40	0.796
Soya	698	2908	43	11,138	822	153	418	0.688
Sugar beet	3923	2543	90	3298	27,467	48	224	0.731
Sunflower	37	267	617	127	63	4427	1032	0.674
Winter crops	310	1580	600	1242	385	4493	109,901	0.927
PA	0.337	0.810	0.683	0.549	0.837	0.441	0.971	
							OA	0.832
							Kappa	0.754

In general, most confusion between winter crops and the other crops can be explained with the sub-optimal timing of the S2 image acquisition (30 August). At this time many of the crops are in an advanced growth stage or already in senescence (Figure 5). Better results can be expected by either choosing a more suitable date for image acquisition or by using multi-temporal data [53–57]. Nevertheless, even using a single (and not perfectly timed) image, the results are already comparable to the outcome of the study presented in Inglada *et al.* [16]. They investigated the classification performance using multi-temporal SPOT images over 12 sites and achieved overall accuracies around 80%–85% for most sites.

Our pixel- or object-based classifications did not show clear differences in terms of accuracy and visual appearance of the maps. Hence, only pixel-based results are presented in Figure 9; the corresponding area statistics are listed in Table 6. Although no (parcel) boundaries were imposed to produce the map shown in Figure 9, field boundaries are well depicted and can be easily recognized. Figure 10 shows the corresponding margin map for the pixel-based classification (in Figure 8 the margins are shown per crop type). Again, very little high-frequency spatial variability (salt-and-pepper) can be observed while a clear spatial structure appears. Areas with low margin often correspond to the classes onion, sunflower and carrots, whereas winter crops and sugar beet are often classified with higher margins.

Table 6. Area statistics (in ha) derived from the pixel-based classification of the cropland test site *Marchfeld*.

Carrots	Maize	Onions	Soya	Sugar Beet	Sunflower	Winter Crops
1198	12,009	798	3302	7040	1943	33,234

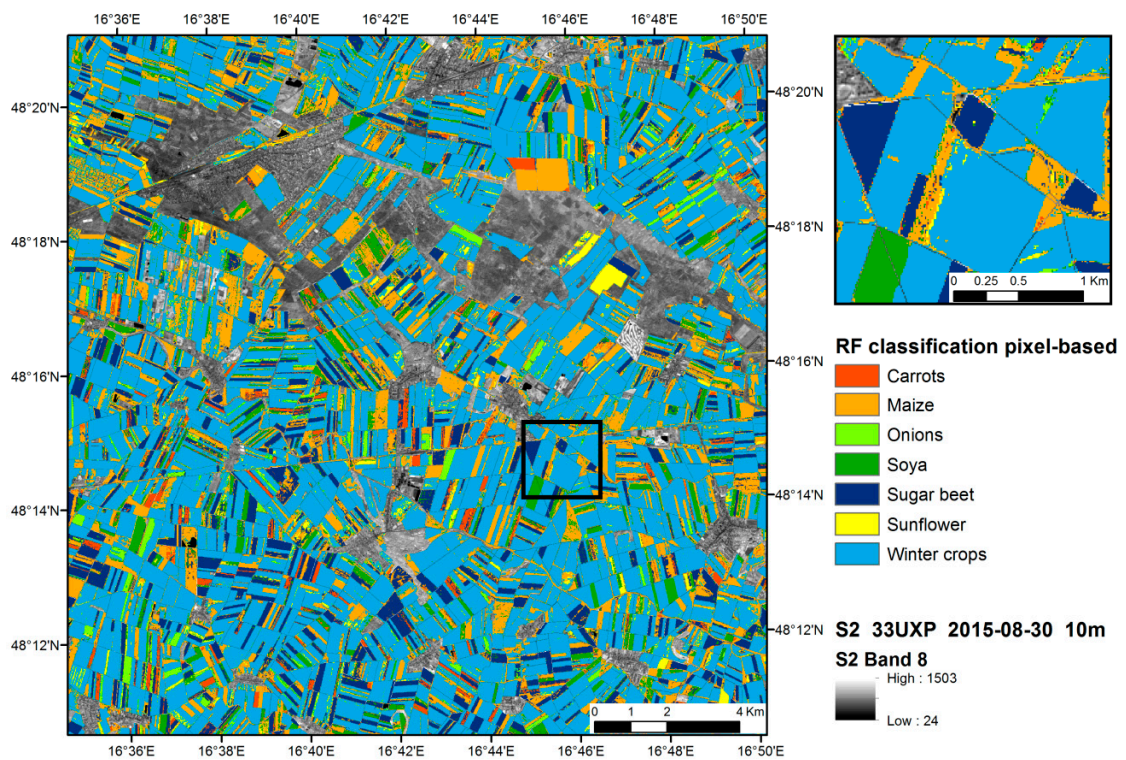


Figure 9. Classification result based on the pixel-based approach for the cropland test site *Marchfeld*. Forest areas were masked out using CORINE Land Cover and OSM layers.

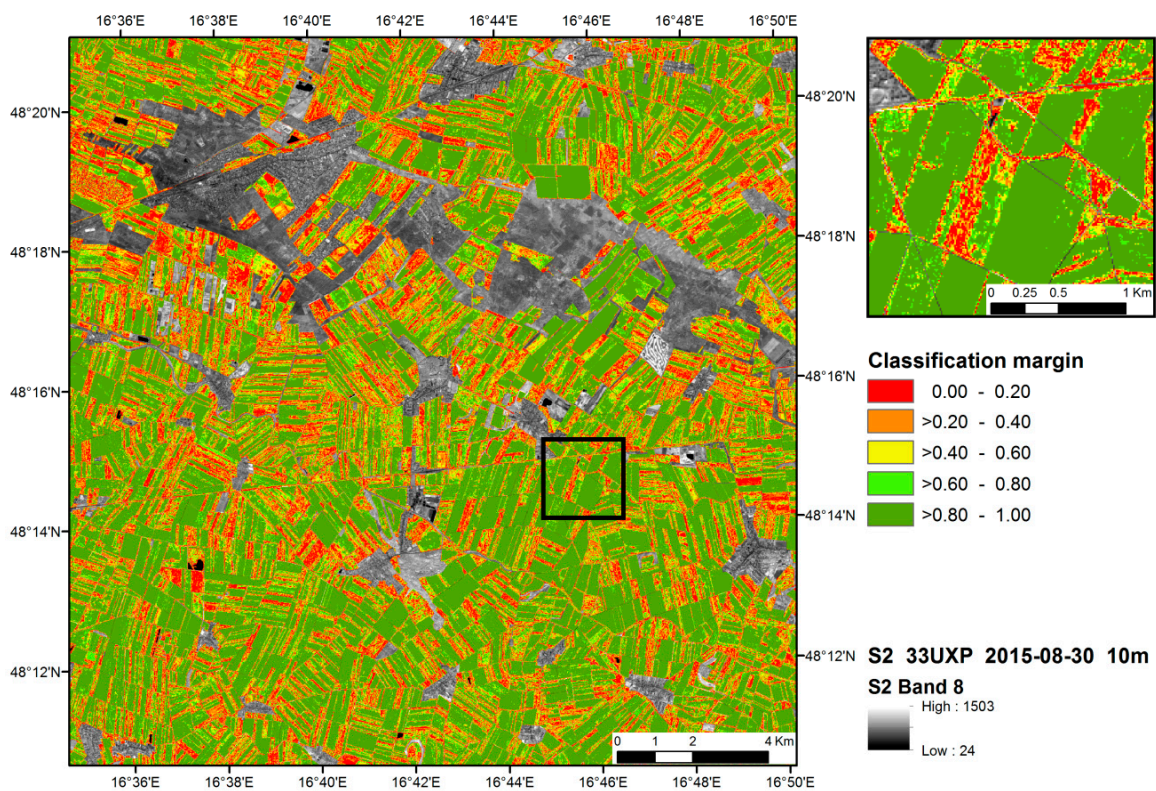


Figure 10. Classification margin of the pixel-based classification of the cropland test site *Marchfeld*. Forest areas were masked out using CORINE Land Cover and OSM layers. A higher margin value indicates a higher classification reliability.

Differences between pixel- or object-based approaches are probably small in our crop classification experiment as crop management creates relatively homogeneous vegetation development conditions. Compared to very high resolution (VHR) data with pixel sizes of about 1 m, textural features are also less well expressed in S2 data with 10 m resolution; the relatively small field sizes in Austria have also to be noted. Together these factors contribute to the sub-optimum performance of the OBIA approach. Insignificant differences between the two classification approaches were also found in [58] based on the analysis of SPOT-5 data at 10 m spatial resolution.

Regarding the importance of the 10 spectral bands, we found large differences in MDA (Figure 11). Amongst the five most important bands, two were located in the red-edge, one in the visible and two in the SWIR spectral region. Interestingly, both NIR bands (8 and 8A) scored very low.

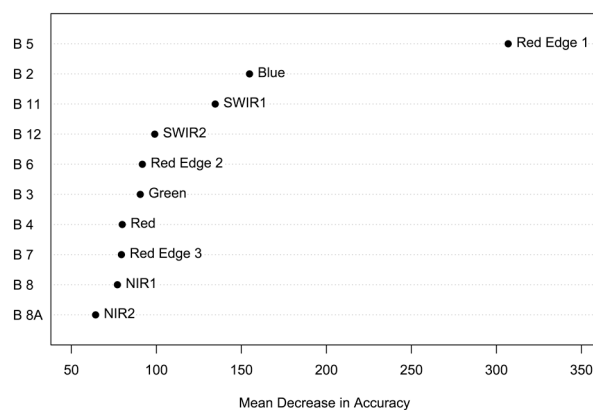


Figure 11. Ranking of spectral bands based on the importance measure MDA (Mean Decrease in Accuracy) obtained from the Random Forest (RF) model for the pixel-based classification using all reference data of the cropland test site *Marchfeld*; a higher score indicates a higher importance.

3.2. Tree Species Classification

At the time of image acquisition, the seven tree species had very similar spectral shapes resulting in large spectral overlaps and often low classification margins (Figure 12). Compared to the spectral signatures of crops (Figure 8), the tree signatures look somewhat featureless and seem simply scaled along the y-axis (e.g., darker/brighter). The high(er) inter-band correlation is also reflected in the relatively uninspired principle components (Figures A2g,h and A2g,h).

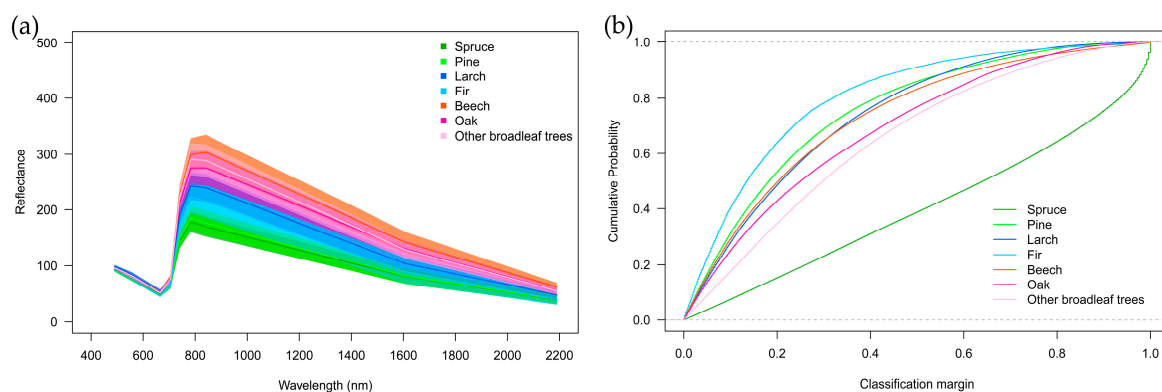


Figure 12. Spectral signatures and classification margins of the seven tree species of the forest test sites *Ebersberg* and *Altoetting*. (a) Spectral signatures including the specific intra-class standard deviations. The Top-of-Atmosphere (ToA) reflectance values (y-axis) are multiplied by a factor of 1000; (b) Classification margins of the seven tree classes displayed as cumulative frequency distributions.

The confusion matrix in Table 7 summarizes the results for the object-based classification of seven forest classes based on a 10-fold cross-validation. The two groups of coniferous and broadleaf trees (shaded areas in Table 7) were nearly perfectly separated (93% correct), whereas class-specific classifications were not always satisfactory. The classification of the most important forest species spruce achieved a producer's accuracy of 85.7% and user's accuracy of 76.7%. In addition, larch, fir and beech reached acceptable accuracy values (60%–70%). The highest misclassification rate was observed for pine: only around 14% of the pine validation samples were correctly classified, but 70% misclassified as spruce. At the time of image acquisition, the two forest classes spruce and pine had a very large spectral overlap across all 10 spectral channels of S2 (Figure 12).

Table 7. Confusion matrix and statistical measures for the object-based tree species classification for the forest test sites *Ebersberg* and *Altoetting*. Results were obtained using 10-fold cross-validation (other BL = other broadleaf trees).

OBJECT-BASED	Spruce	Pine	Larch	Fir	Beech	Oak	Other BL	UA
Spruce	66	15	2	3	0	0	0	0.767
Pine	1	3	1	0	0	0	0	0.600
Larch	5	2	28	1	0	2	6	0.636
Fir	4	0	1	20	1	0	2	0.714
Beech	0	0	0	0	48	8	9	0.738
Oak	1	1	2	0	2	7	2	0.467
Other BL	0	0	4	2	15	15	38	0.514
PA	0.857	0.143	0.737	0.769	0.727	0.219	0.667	
							OA	0.662
							Kappa	0.588

The results of the pixel-based classification for the forest test sites are presented in Table 8. Compared to the object-based approach (Table 7), the pixel-based classification gave a slightly lower overall accuracy. In particular, the class specific results were significantly worse in the pixel-based approach, except for spruce (nearly the same accuracy), pine and oak (better results). The highest decrease in accuracy was observed for fir and larch. We also observe a lower kappa coefficient compared to the object-based approach.

Table 8. Confusion matrix and statistical measures for the pixel-based tree species classification for the forest test sites *Ebersberg* and *Altoetting*. Results were obtained using 10-fold cross-validation (other BL = other broadleaf trees).

PIXEL-BASED	Spruce	Pine	Larch	Fir	Beech	Oak	Other BL	UA
Spruce	75,563	26,496	310	327	21	220	203	0.733
Pine	12,616	6867	88	135	21	275	146	0.341
Larch	60	180	748	2	35	60	343	0.524
Fir	77	16	3	183	2	0	7	0.635
Beech	11	8	24	10	3406	1761	2030	0.470
Oak	107	233	92	32	1713	3653	2480	0.440
Other BL	173	262	435	71	1779	2827	6555	0.542
PA	0.853	0.202	0.440	0.241	0.488	0.415	0.557	
							OA	0.635
							Kappa	0.357

Both tree species classifications are therefore not fully satisfactory. In general, the achieved classification accuracies are lower than those of other studies, in which satellite data with higher spatial resolution were used (e.g., WorldView-2) [17,59].

A main reason for the observed difficulties results from the fact that the selected forests are characterized by a heterogeneous and highly fragmented species distribution. Consequently, lower

classification accuracies were observed for those tree species which are either rare in the study area or seldom form pure stands. For these tree classes, the delimitation of suitable reference data was already difficult. The spatial resolution of S2 has to be taken into account for future field work and reference data acquisition [60]. The lower producer accuracies for larch and fir for example, are due to the smaller size of the available reference polygons (Table 2). The classification results are often better for the dominant classes. This is more evident in the pixel-based approach because larger polygons (reference data) imply more reference pixels for the model generation. For a more detailed comparison of the two approaches, these differences should be taken into account using alternative methods such as proposed by Radoux and Bogaert [61]. Additionally it has to be considered that the forest classes are more heterogeneous than the cropland classes. Parameters such as age, stand density, crown coverage and understory have a direct influence on the spectral behavior of forest classes and their intra-class variability [62,63]. Forest canopies show a very complex surface with an alternation of well-illuminated and shaded parts. This should in principle favor the use of object-based approaches [17,64,65]. In our case, however, object sizes were relatively small compared to the spatial resolution of S2, and this in particular for the non-dominant species (Table 2). Therefore, the theoretical advantages of OBIA could not play out as well as for EO data with a very high spatial resolution [17,59,65–68]. Instead, in our case, the two approaches obtained comparable overall accuracies. Only the kappa coefficient showed a (clear) advantage of the object-based approach.

The maps in Figure 13 and Table 9 correctly show the dominance of spruce in both forest test sites. Together with the higher amount of pine in the *Altoetting* area, these results are in line with forest descriptions of the forest enterprise [31]. However, some of the pure pine stands in the southwest part of the *Altoetting* study site are in reality mixed stands with spruce. In addition, the high amount of other broadleaf trees seems to be too high, even if the dominance in the riverbank vegetation is plausible. This class and the oak class are over-classified at the cost of beech. Although the spatial resolution of S2 is not fine enough for the delineation and classification of individual tree crowns, the maps show the potential to classify even heterogonous forests, mainly if the stand composition is not on individual tree level but at the level of tree groups.

As expected, the classification margin shows tree specific differences. Classes which show higher classification accuracies like spruce (Table 8), obtained also higher values for the classification margin (Figures 12 and 14).

Amongst the five most important spectral bands, we found two in the SWIR (B11 and B12), one in the red-edge (B5) and two in the visible (B2, B4) (Figure 15). Hence, compared to the crop classification (Figure 11), a similar set of “best” spectral bands was identified. In particular, the three “best” spectral channels were identical in both studies (e.g., B2, B5 and B11). RGB false color composites of blue (B2), Red Edge-1 (B5) and SWIR-1 (B11) for all test sites are shown in Appendix A (Figure A2a–Figure A2f).

Table 9. Area statistics (in ha) derived from the pixel-based classification of the forest test sites *Ebersberg* and *Altoetting*.

Spruce	Pine	Larch	Fir	Beech	Oak	Other BL
17,626	3050	2006	125	3456	5551	12,332

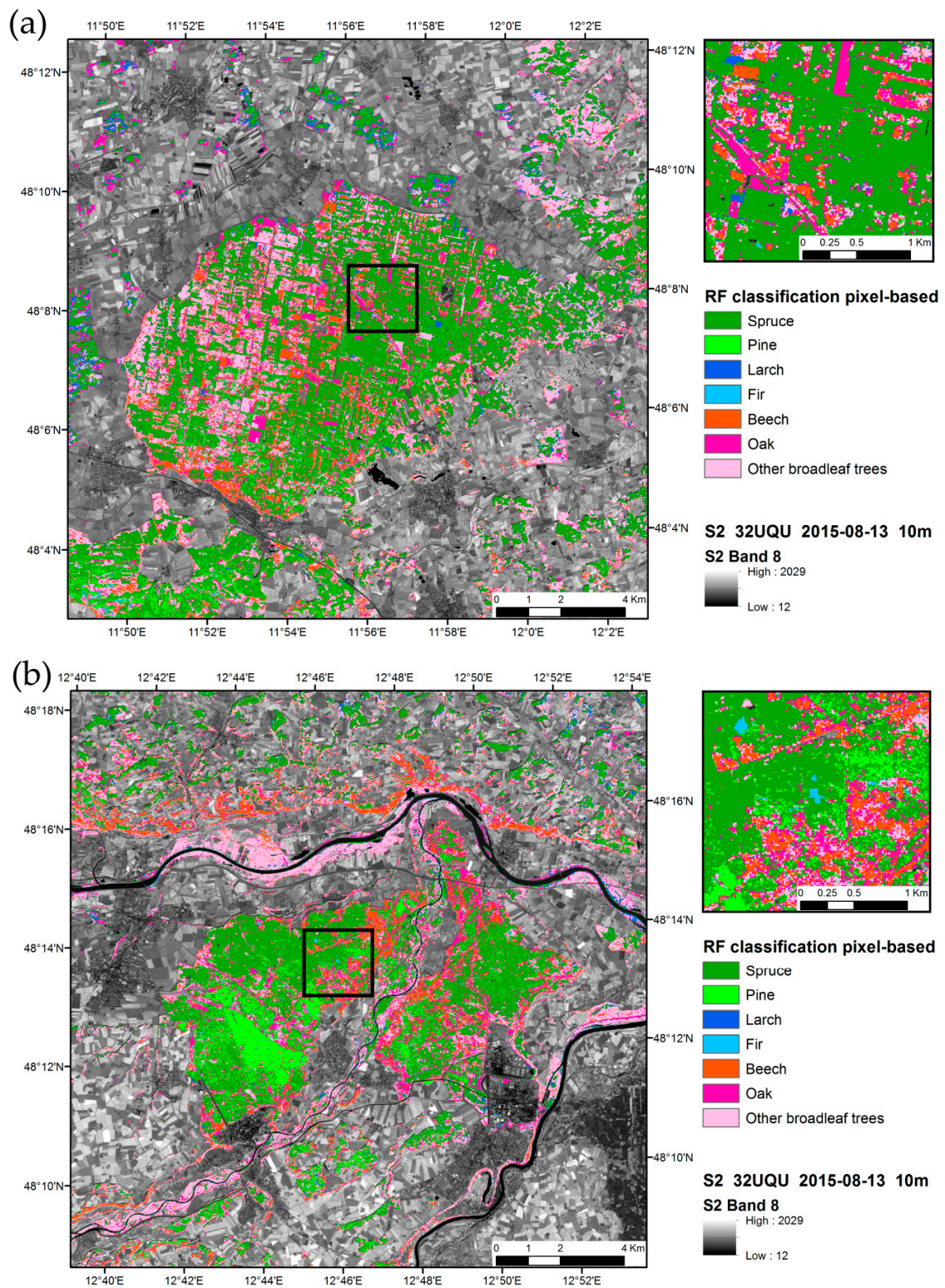


Figure 13. Classification result based on the pixel-based approach for the two forest test sites (a) Ebersberg and (b) Altoetting.

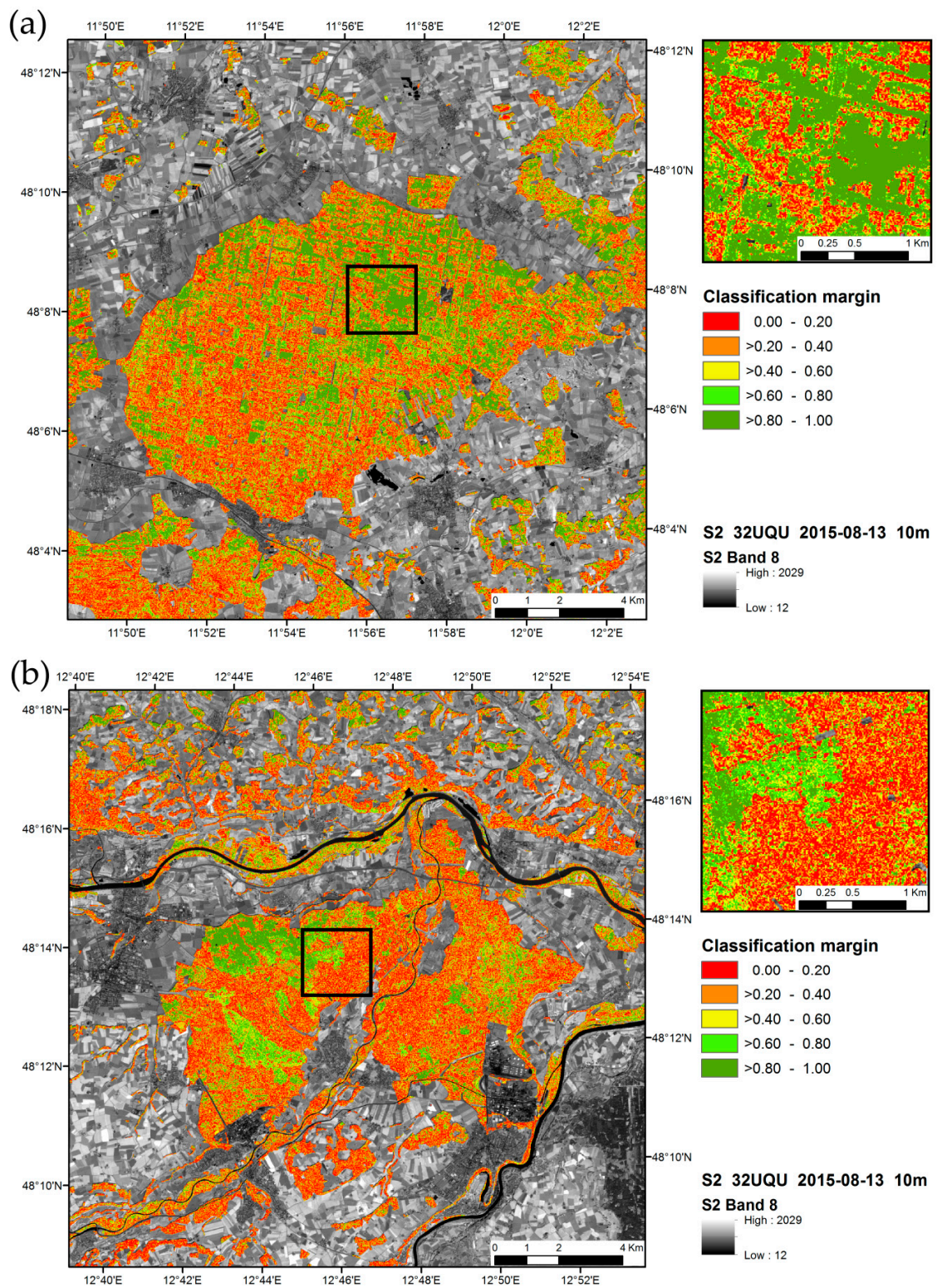


Figure 14. Classification margin of the pixel-based classification of the two forest test sites (a) *Ebersberg* and (b) *Altoetting*. A higher margin value indicates a higher classification reliability.

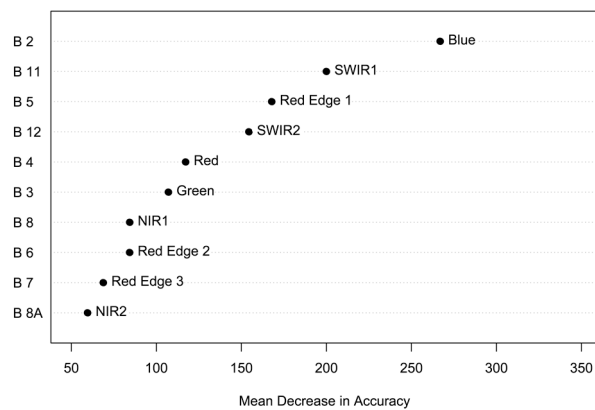


Figure 15. Ranking of spectral bands based on the importance measure MDA (Mean Decrease in Accuracy) obtained from the Random Forest (RF) model for the pixel-based classification based on all reference data of the forest test sites *Ebersberg* and *Altoetting*; a higher score indicates a higher importance.

3.3. Potential of Sentinel-2 for Vegetation Classification

Despite non-optimal acquisition times, the classification results confirmed the high potential of S2 data to derive specific crop type and tree species maps. In this respect it has to be considered that the analyzed data was released by ESA as “pre-operational” and still showed some artifacts. These artifacts will be corrected during the coming months. Although qualified as “pre-operational”, the analyzed Sentinel-2 scenes were nevertheless of high quality. In particular, a comparison against existing satellite images from Landsat-8, Deimos-1 and SPOT-5, acquired in the same period, revealed a very good spatial and spectral agreement (not shown).

Object-based classifications achieved cross-validated overall accuracies (OA) of 76.8% for crop types and of 66.2% for tree species identification. In both case studies, we could not find distinct advantages using an object-based image analysis (OBIA) compared to a classical pixel-based classification. For example, the pixel-based approach yielded slightly better overall accuracies for cropland (OA = 83.2%) and lower accuracies for forests (OA = 63.5%). This finding was mainly related to the fact that some of the objects created using the LSMS segmentation were relatively small. Small objects mainly resulted from the highly fragmented forests, respectively, the small agricultural fields in the cropland area. Even with the 10 m pixel size of S2, the extraction of meaningful textural features *etc.* from small objects is not possible. Hence, textural information could not contribute to higher classification accuracies [38,69,70].

Regarding the spectral information, both case studies confirmed the high value of the red-edge and shortwave infrared (SWIR) bands for vegetation mapping fully in line with other studies [45,71,72]. The blue band was also important in both studies. Surprisingly, the S2-bands in the near infrared were amongst the least important channels. Although interesting, these findings have to be considered with caution as only one set of image was analyzed and other bands might be of high importance in different landscapes and/or using images acquired in other season(s). Further research is warranted to address these issues.

Most confusion in our crop type and tree species maps was due to the non-optimum timing of the S2 acquisitions. For our study, only images acquired (mid/end) of August were available. Such late acquisitions are certainly not optimal for distinguishing crop types as most crops are already in an advanced stage of development or even in senescence. Also for forest classifications, images acquired earlier (end of spring) or later (beginning of autumn) in the year would probably lead to higher classification accuracies. For all land cover types, we expect higher classification accuracies with better timing of the acquisitions and in particular by using multi-temporal data [57,73–75].

Regarding the spatial information, crop classifications were applied using the S2 bands (excluding B1, B9 and B10) resampled at either 10 or 20 m pixels size. We reported here only the findings from the layer stack at 10 m resolution as no differences were observed in terms of thematic accuracy between 10 and 20 m. In the case of the tree species classifications, however, it was already difficult to identify and delineate pure forests stands at 10 m spatial resolution. Therefore, we combined in a layer stack the four S2 bands at 10 m and the six bands at 20 m by resampling the latter at 10 m pixel size. We confirm the finding of Stratoulia *et al.* [14] that the spatial resolution of S2 (in particular the bands with 20 m GSD) could be too low for mapping very highly fragmented forests and landscapes. As a spatial resolution of 10 m is not sufficient to capture single trees [19], a very detailed description of forests with a high amount of species based on S2 data seems to be difficult. Therefore, we recommend combining dense time series from S2 with rich spectral information and very high spatial resolution images (e.g., orthophotos). Very high resolution (VHR) images would probably also positively contribute to the extraction of textural attributes.

Sentinel-2 was specifically designed to collect dense time series. The mission plan from ESA foresees two identical satellites in operation (S2A and S2B). With the second Sentinel-2 (S2B launch expected in June 2016), the S2 constellation will achieve a revisit time of 5 days. Within the overlap areas, even higher revisit times will be possible. The temporal frequency of cloud-free acquisitions will be further increased as S2 was designed for building a virtual constellation with Landsat-8 with a high potential for global monitoring [76]. Hence, compared to our study, much more data will be freely available in the near future, which will significantly impact the capturing of land cover/land use (LCLU) information [21]. Despite the few data analyzed in our study, our research demonstrated that even using a single image, crop classification accuracies can be achieved comparable to the outcome of the study presented in Inglada *et al.* [16].

4. Conclusions

In this study, the performance of pre-operational Sentinel-2 (S2) data to derive crop type and tree species maps was analyzed in Austria (for cropland) and Germany (for forests). In both case studies, only single cloud-free S2 scenes were used (both acquired in August 2015). Using the mono-temporal datasets, we applied a Random Forest classifier (RF) using supervised pixel- and object-based classifications. We used as inputs 10 spectral bands of S2 resampled to 10 m pixel size. The classification models were validated using a 10-fold cross-validation approach. Data for training and validation were collected from field survey (cropland), respectively from forest inventory data and visual interpretation of very high spatial resolution images (forests).

The achieved classifications results for the pixel- and the object-based approach were satisfactory but not extremely high. It is not known how much the “pre-operational” status of the analyzed images contributed to the observed misclassifications. Certainly, with the current refinements done by ESA and its partners, it can be expected that the data quality will further increase. Likewise, a better timing of the acquisition will improve the classification results. The use of multi-temporal S2 data has probably the highest potential for further increasing classification results. In the future, with the two twin S2 satellites in orbit, dense time series will be available. Albeit S2’s spatial resolution of 10 and 20 m imposes some limitations for very detailed analyses, the potential of data with this level of spatial detail, its well-chosen spectral bands and global coverage, is unprecedented.

Acknowledgments: We greatly acknowledge ESA’s support for this study by providing early access to pre-operational Sentinel-2 data. We thank in particular Bianca Hoersch (ESA) and her team for having invited us to be part of ESA’s S2A Expert User technical session and the provided support. We further thank BaySF and LWF for access to forest inventory data.

Author Contributions: Markus Immitzer, Francesco Vuolo and Clement Atzberger conceived and designed the study; Markus Immitzer and Francesco Vuolo performed the data processing; Markus Immitzer, Francesco Vuolo and Clement Atzberger analyzed the results and wrote the paper.

Conflicts of Interest: The authors declare no conflict of interest.

Abbreviations

The following abbreviations are used in this manuscript:

ATKIS	Amtliches Topographisch-Kartographische Informationssystem
BL	broadleaf trees
CORINE	Coordination of Information on the Environment
GSD	Ground Sampling Distance
LCLU	Land Cover and Land Use
LSMS	Large Scale Mean Shift
MDA	Mean Decrease in Accuracy
MSI	Multi-Spectral Imager
NIR	Near Infrared
OA	Overall Accuracy
OBIA	Object Based Image Analysis
OSM	Open Street Map
PA	Producer's Accuracy
PC	Principle Component
PCA	Principle Component Analysis
RF	Random Forest
S2	Sentinel-2
SWIR	Shortwave Infrared
ToA	Top-of-Atmosphere
UA	User's accuracy

Appendix A

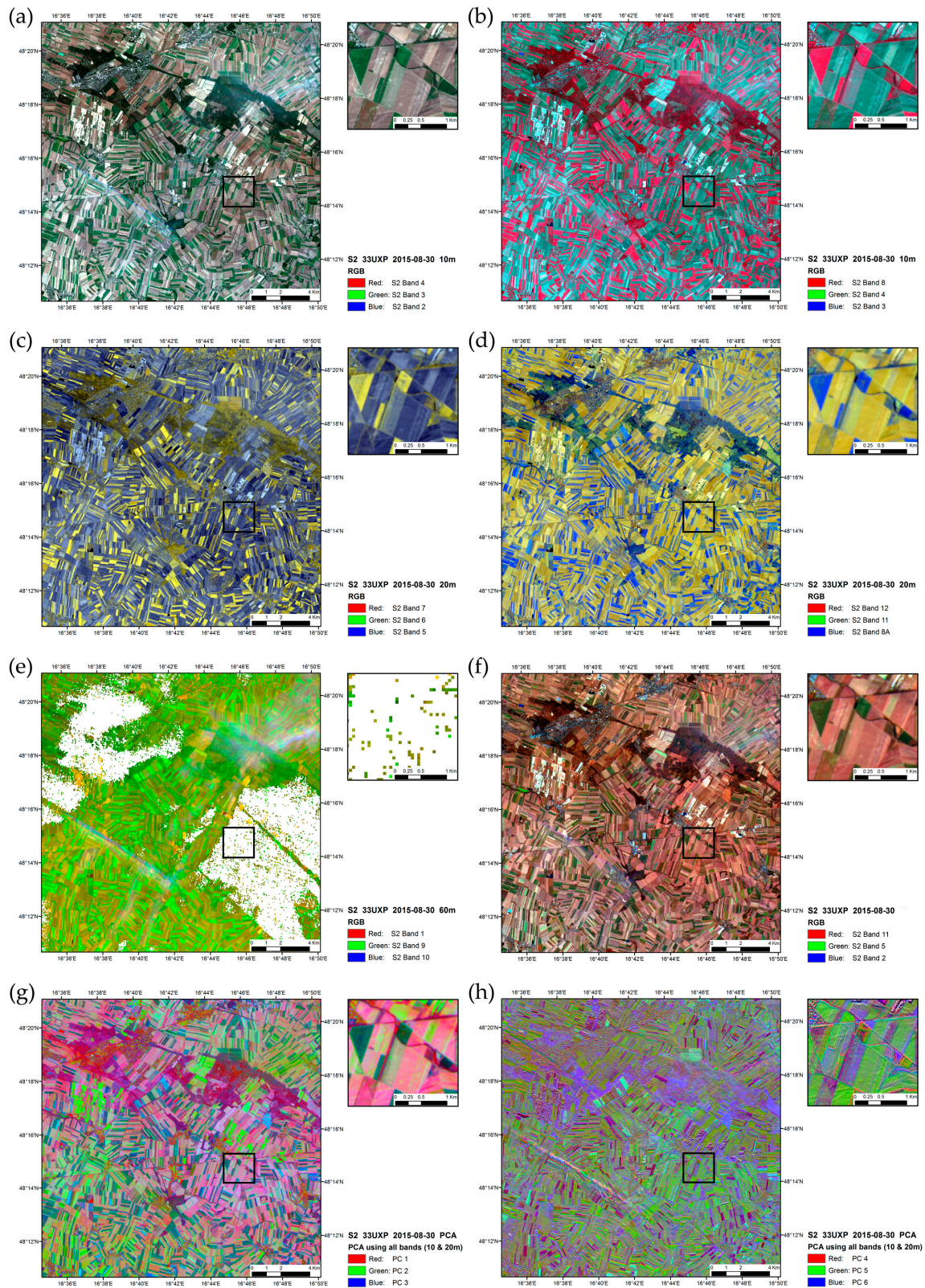


Figure A1. Sentinel-2 scene (30 August 2015) of the cropland test site *Marchfeld*, Austria. Different band combinations and PCA results (Number indicates the used data for R,G,B): (a) 10 m bands 4,3,2; (b) 10 m bands 8,4,3; (c) 20 m bands 7,6,5; (d) 20 m bands 12,11,8A; (e) 60 m bands 1,9,10; (f) 20 m bands 11,5,2; (g) PC1, PC2, PC3; (h) PC4, PC5, PC6.

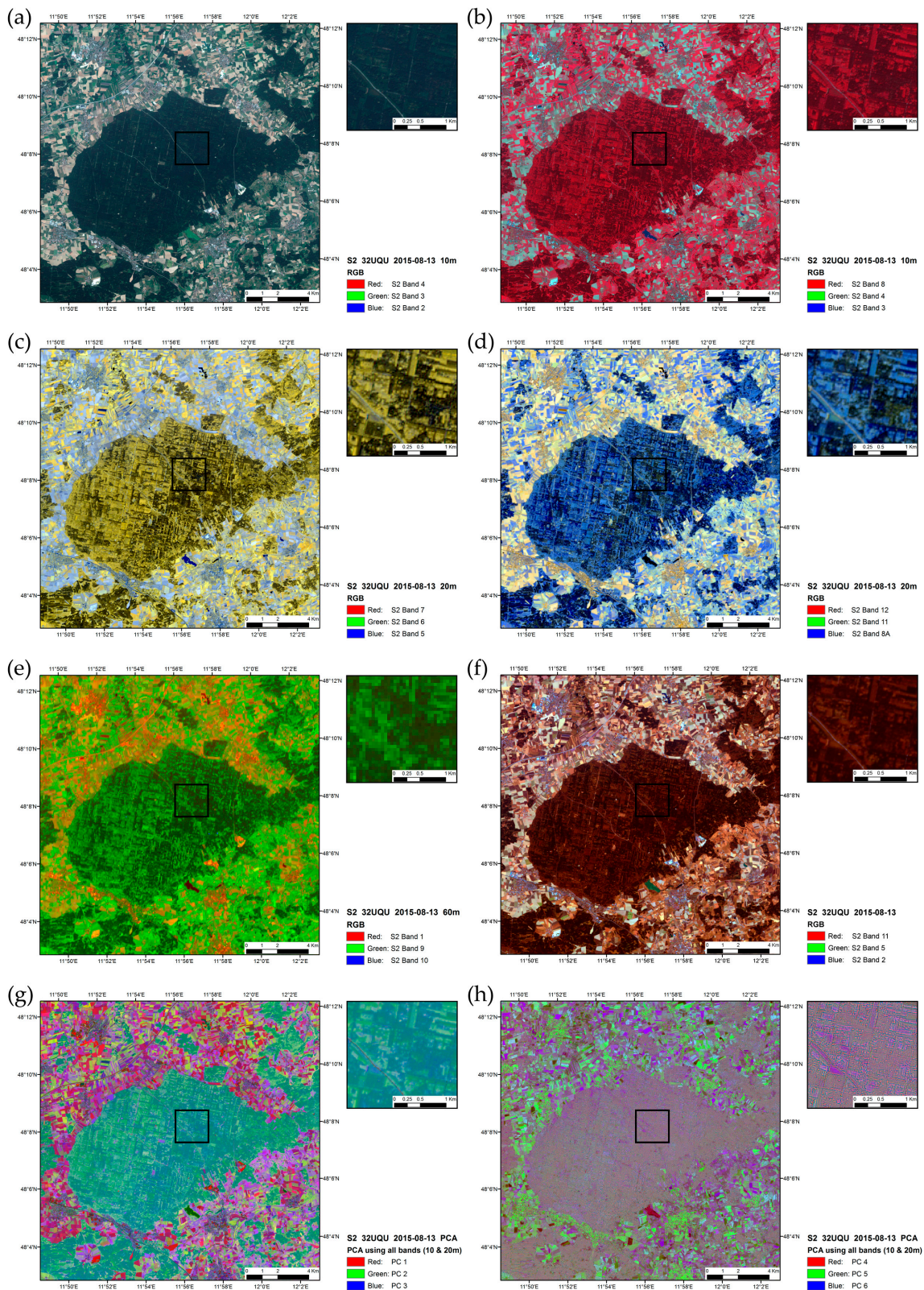


Figure A2. Sentinel-2 scene (13 August 2015) of the first forest test site *Ebersberg* in Bavaria, Germany. Different band combinations and PCA results (Number indicates the used data for R,G,B): (a) 10 m bands 4,3,2; (b) 10 m bands 8,4,3; (c) 20 m bands 7,6,5; (d) 20 m bands 12,11,8A; (e) 60 m bands 1,9,10; (f) 20 m bands 11,5,2; (g) PC1, PC2, PC3; (h) PC4, PC5, PC6.

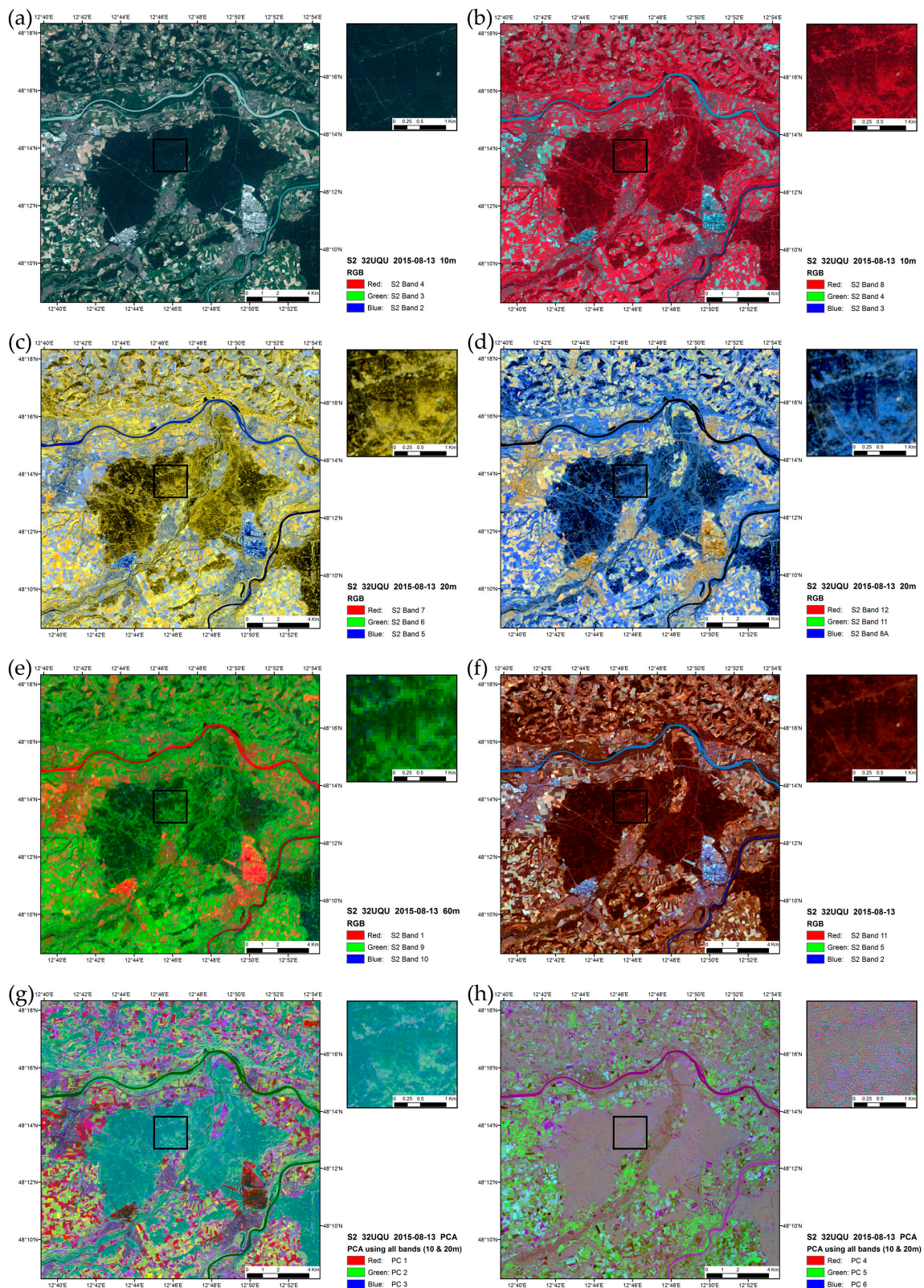


Figure A3. Sentinel-2 scene (13 August 2015) of the second forest test site *Altoetting* in Bavaria, Germany. Different band combinations and PCA results (Number indicates the used data for R,G,B): (a) 10 m bands 4,3,2; (b) 10 m bands 8,4,3; (c) 20 m bands 7,6,5; (d) 20 m bands 12,11,8A; (e) 60 m bands 1,9,10; (f) 20 m bands 11,5,2; (g) PC1, PC2, PC3; (h) PC4, PC5, PC6.

References

1. ESA Sentinel-2 Delivers First Images. Available online: http://www.esa.int/Our_Activities/Observing_the_Earth/Copernicus/Sentinel-2/Sentinel-2_delivers_first_images (accessed on 7 January 2016).
2. Drusch, M.; Del Bello, U.; Carlier, S.; Colin, O.; Fernandez, V.; Gascon, F.; Hoersch, B.; Isola, C.; Laberinti, P.; Martimort, P.; et al. Sentinel-2: ESA's Optical High-Resolution Mission for GMES Operational Services. *Remote Sens. Environ.* **2012**, *120*, 25–36. [[CrossRef](#)]
3. ESA Introducing Sentinel-2. Available online: http://www.esa.int/Our_Activities/Observing_the_Earth/Copernicus/Sentinel-2/Introducing_Sentinel-2 (accessed on 17 December 2015).
4. Malenovský, Z.; Rott, H.; Cihlar, J.; Schaepman, M.E.; García-Santos, G.; Fernandes, R.; Berger, M. Sentinels for science: Potential of Sentinel-1, -2 and -3 missions for scientific observations of ocean, cryosphere, and land. *Remote Sens. Environ.* **2012**, *120*, 91–101. [[CrossRef](#)]
5. Agapiou, A.; Alexakis, D.D.; Sarris, A.; Hadjimitsis, D.G. Evaluating the Potentials of Sentinel-2 for Archaeological Perspective. *Remote Sens.* **2014**, *6*, 2176–2194. [[CrossRef](#)]
6. Clasen, A.; Somers, B.; Pipkins, K.; Tits, L.; Segl, K.; Brell, M.; Kleinschmit, B.; Spengler, D.; Lausch, A.; Förster, M. Spectral unmixing of forest crown components at close range, airborne and simulated Sentinel-2 and EnMAP spectral imaging scale. *Remote Sens.* **2015**, *7*, 15361–15387. [[CrossRef](#)]
7. Clevers, J.G.P.W.; Gitelson, A.A. Remote estimation of crop and grass chlorophyll and nitrogen content using red-edge bands on Sentinel-2 and -3. *Int. J. Appl. Earth. Obs. Geoinf.* **2013**, *23*, 344–351. [[CrossRef](#)]
8. Dong, T.; Meng, J.; Shang, J.; Liu, J.; Wu, B. Evaluation of Chlorophyll-Related Vegetation Indices Using Simulated Sentinel-2 Data for Estimation of Crop Fraction of Absorbed Photosynthetically Active Radiation. *IEEE J. Sel. Top. Appl. Earth Obs. Remote Sens.* **2015**, *8*, 4049–4059. [[CrossRef](#)]
9. Dotzler, S.; Hill, J.; Buddenbaum, H.; Stoffels, J. The Potential of EnMAP and Sentinel-2 Data for Detecting Drought Stress Phenomena in Deciduous Forest Communities. *Remote Sens.* **2015**, *7*, 14227–14258. [[CrossRef](#)]
10. Frampton, W.J.; Dash, J.; Watmough, G.; Milton, E.J. Evaluating the capabilities of Sentinel-2 for quantitative estimation of biophysical variables in vegetation. *ISPRS J. Photogramm. Remote Sens.* **2013**, *82*, 83–92. [[CrossRef](#)]
11. Hill, M.J. Vegetation index suites as indicators of vegetation state in grassland and savanna: An analysis with simulated SENTINEL 2 data for a North American transect. *Remote Sens. Environ.* **2013**, *137*, 94–111. [[CrossRef](#)]
12. Richter, K.; Hank, T.B.; Vuolo, F.; Mauser, W.; D'Urso, G. Optimal Exploitation of the Sentinel-2 Spectral Capabilities for Crop Leaf Area Index Mapping. *Remote Sens.* **2012**, *4*, 561–582. [[CrossRef](#)]
13. Sibanda, M.; Mutanga, O.; Rouget, M. Examining the potential of Sentinel-2 MSI spectral resolution in quantifying above ground biomass across different fertilizer treatments. *ISPRS J. Photogramm. Remote Sens.* **2015**, *110*, 55–65. [[CrossRef](#)]
14. Stratoulis, D.; Balzter, H.; Sykioti, O.; Zlinszky, A.; Tóth, V.R. Evaluating sentinel-2 for lakeshore habitat mapping based on airborne hyperspectral data. *Sens. Switz.* **2015**, *15*, 22956–22969. [[CrossRef](#)] [[PubMed](#)]
15. Van der Meer, F.D.; van der Werff, H.M.A.; van Ruitenbeek, F.J.A. Potential of ESA's Sentinel-2 for geological applications. *Remote Sens. Environ.* **2014**, *148*, 124–133. [[CrossRef](#)]
16. Inglada, J.; Arias, M.; Tardy, B.; Hagolle, O.; Valero, S.; Morin, D.; Dedieu, G.; Sepulcre, G.; Bontemps, S.; Defourny, P.; Koetz, B. Assessment of an Operational System for Crop Type Map Production Using High Temporal and Spatial Resolution Satellite Optical Imagery. *Remote Sens.* **2015**, *7*, 12356–12379. [[CrossRef](#)]
17. Immitzer, M.; Atzberger, C.; Koukal, T. Tree species classification with Random Forest using very high spatial resolution 8-band WorldView-2 satellite data. *Remote Sens.* **2012**, *4*, 2661–2693. [[CrossRef](#)]
18. Nagendra, H. Using remote sensing to assess biodiversity. *Int. J. Remote Sens.* **2001**, *22*, 2377–2400. [[CrossRef](#)]
19. Wulder, M.A.; Hall, R.J.; Coops, N.C.; Franklin, S.E. High spatial resolution remotely sensed data for ecosystem characterization. *BioScience* **2004**, *54*, 511–521. [[CrossRef](#)]
20. Banskota, A.; Kayastha, N.; Falkowski, M.J.; Wulder, M.A.; Froese, R.E.; White, J.C. Forest Monitoring Using Landsat Time Series Data: A Review. *Can. J. Remote Sens.* **2014**, *40*, 362–384. [[CrossRef](#)]
21. Wulder, M.A.; Coops, N.C. Satellites: Make Earth observations open access. *Nature* **2014**, *513*, 30–31. [[CrossRef](#)] [[PubMed](#)]
22. Asner, G.P. Geography of forest disturbance. *Proc. Natl. Acad. Sci.* **2013**, *110*, 3711–3712. [[CrossRef](#)] [[PubMed](#)]

23. Kohavi, R. A study of cross-validation and bootstrap for accuracy estimation and model selection. In *International Joint Conference on Artificial Intelligence*; 1995; Volume 14, pp. 1137–1145.
24. EEA Corine Land Cover 2000 Raster Data. Available online: <http://www.eea.europa.eu/data-and-maps/data/corine-land-cover-2000-raster-3> (accessed on 7 January 2016).
25. Adv Amtliches Topographisch-Kartographisches Informationssystem (ATKIS). Available online: <http://www.adv-online.de/AAA-Modell/ATKIS/> (accessed on 7 January 2016).
26. *EC Copernicus Europe's Eyes on Earth*; Copernicus Brochure; European Commission: Brussels, B, 2015. Available online: http://www.esa.int/Our_Activities/Observing_the_Earth/Copernicus/Overview4 (accessed on 27 October 2015).
27. Eitzinger, J.; Kersebaum, K.C.; Formayer, H. *Landwirtschaft im Klimawandel: Auswirkungen und Anpassungsstrategien für die Land- und Forstwirtschaft in Mitteleuropa*; Agrimedia: Clenze, Germany, 2009.
28. Thaler, S.; Eitzinger, J.; Dubrovský, M.; Trnka, M. Climate change impacts on selected crops in Marchfeld, Eastern Austria. In *Proceedings of the 28th Conference on Agricultural and Forest Meteorology*, Orlando, FL, USA, 28 April–2 May 2008.
29. Rischbeck, P. Der Einfluss von Klimaänderung, Bodenbearbeitung und Saattermin auf den Wasserhaushalt und das Ertragspotential von Getreide im Marchfeld. Ph.D. Thesis, University of Natural Resources and Life Sciences, Vienna (BOKU), Vienna, Austria, September 2007.
30. Neugebauer, N.; Vuolo, F. Crop water requirements on regional level using remote sensing data—A case study in the Marchfeld Region. *Photogramm. Fernerkund. Geoinformation*. **2014**, *2014*, 369–381. [[CrossRef](#)]
31. BaySF. *Regionales Naturschutzkonzept für den Forstbetrieb Wasserburg am Inn*; Bayerische Staatsforsten Forstbetrieb Wasserburg: Wasserburg, Germany, 2013; p. 65. Available online: http://www.baysf.de/fileadmin/user_upload/01-ueber_uns/05-standorte/FB_Wasserburg_a._Inn/Naturschutzkonzept_Wasserburg.pdf (accessed on 15 December 2015).
32. Fukunaga, K.; Hostetler, L. The estimation of the gradient of a density function, with applications in pattern recognition. *IEEE Trans. Inf. Theory* **1975**, *21*, 32–40. [[CrossRef](#)]
33. Comaniciu, D.; Meer, P. Mean shift: A robust approach toward feature space analysis. *IEEE Trans. Pattern Anal. Mach. Intell.* **2002**, *24*, 603–619. [[CrossRef](#)]
34. Ming, D.; Ci, T.; Cai, H.; Li, L.; Qiao, C.; Du, J. Semivariogram-Based Spatial Bandwidth Selection for Remote Sensing Image Segmentation With Mean-Shift Algorithm. *IEEE Geosci. Remote Sens. Lett.* **2012**, *9*, 813–817. [[CrossRef](#)]
35. Michel, J.; Youssefi, D.; Grizonnet, M. Stable Mean-Shift Algorithm and Its Application to the Segmentation of Arbitrarily Large Remote Sensing Images. *IEEE Trans. Geosci. Remote Sens.* **2015**, *53*, 952–964. [[CrossRef](#)]
36. Breiman, L. Random forests. *Mach. Learn.* **2001**, *45*, 5–32. [[CrossRef](#)]
37. Liaw, A.; Wiener, M. Classification and regression by randomForest. *R News* **2002**, *2*, 18–22.
38. Toscani, P.; Immitzer, M.; Atzberger, C. Texturanalyse mittels diskreter Wavelet Transformation für die objektbasierte Klassifikation von Orthophotos. *Photogramm. Fernerkund. Geoinformation*. **2013**, *2*, 105–121. [[CrossRef](#)]
39. Genuer, R.; Poggi, J.-M.; Tuleau-Malot, C. Variable selection using random forests. *Pattern Recognit. Lett.* **2010**, *31*, 2225–2236. [[CrossRef](#)]
40. Gislason, P.O.; Benediktsson, J.A.; Sveinsson, J.R. Random Forests for land cover classification. *Pattern Recognit. Lett.* **2006**, *27*, 294–300. [[CrossRef](#)]
41. Hastie, T.; Tibshirani, R.; Friedman, J. *The Elements of Statistical Learning: Data Mining, Inference, and Prediction*, 2nd ed.; Springer: New York, NY, USA, 2009.
42. Rodríguez-Galiano, V.F.; Chica-Olmo, M.; Abarca-Hernandez, F.; Atkinson, P.M.; Jeganathan, C. Random Forest classification of Mediterranean land cover using multi-seasonal imagery and multi-seasonal texture. *Remote Sens. Environ.* **2012**, *121*, 93–107. [[CrossRef](#)]
43. Conrad, C.; Rahmann, M.; Machwitz, M.; Stulina, G.; Paeth, H.; Dech, S. Satellite based calculation of spatially distributed crop water requirements for cotton and wheat cultivation in Fergana Valley, Uzbekistan. *Glob. Planet. Change* **2013**, *110* (Part A), 88–98. [[CrossRef](#)]
44. Immitzer, M.; Atzberger, C. Early Detection of Bark Beetle Infestation in Norway Spruce (*Picea abies*, L.) using WorldView-2 Data. *Photogramm. Fernerkund. Geoinformation*. **2014**, *2014*, 351–367. [[CrossRef](#)]

45. Schultz, B.; Immitzer, M.; Formaggio, A.R.; Sanches, I.D.A.; Luiz, A.J.B.; Atzberger, C. Self-Guided Segmentation and Classification of Multi-Temporal Landsat 8 Images for Crop Type Mapping in Southeastern Brazil. *Remote Sens.* **2015**, *7*, 14482–14508. [[CrossRef](#)]
46. Pal, M. Random forest classifier for remote sensing classification. *Int. J. Remote Sens.* **2005**, *26*, 217–222. [[CrossRef](#)]
47. Immitzer, M.; Stepper, C.; Böck, S.; Straub, C.; Atzberger, C. Use of WorldView-2 stereo imagery and National Forest Inventory data for wall-to-wall mapping of growing stock. *For. Ecol. Manag.* **2016**, *359*, 232–246. [[CrossRef](#)]
48. Stepper, C.; Straub, C.; Pretzsch, H. Using semi-global matching point clouds to estimate growing stock at the plot and stand levels: application for a broadleaf-dominated forest in central Europe. *Can. J. For. Res.* **2015**, *45*, 111–123. [[CrossRef](#)]
49. R Core Team. *R: A Language and Environment for Statistical Computing*; R Foundation for Statistical Computing: Vienna, Austria, 2015. Available online: <https://www.R-project.org/> (accessed on 10 December 2015).
50. Diaz-Uriarte, R.; Alvarez de Andres, S. Gene selection and classification of microarray data using Random Forest. *BMC Bioinformatics* **2006**, *7*, 3. [[CrossRef](#)] [[PubMed](#)]
51. Foody, G.M. Status of land cover classification accuracy assessment. *Remote Sens. Environ.* **2002**, *80*, 185–201. [[CrossRef](#)]
52. Vuolo, F.; Atzberger, C. Improving land cover maps in areas of disagreement of existing products using NDVI time series of MODIS—Example for Europe. *Photogramm. Fernerkund. Geoinformation.* **2014**, *2014*, 393–407. [[CrossRef](#)]
53. Beyer, F.; Jarmer, T.; Siegmann, B. Identification of Agricultural Crop Types in Northern Israel using Multitemporal RapidEye Data. *Photogramm. Fernerkund. Geoinformation.* **2015**, *2015*, 21–32. [[CrossRef](#)]
54. Conrad, C.; Dech, S.; Dubovyk, O.; Fritsch, S.; Klein, D.; Löw, F.; Schorcht, G.; Zeidler, J. Derivation of temporal windows for accurate crop discrimination in heterogeneous croplands of Uzbekistan using multitemporal RapidEye images. *Comput. Electron. Agric.* **2014**, *103*, 63–74. [[CrossRef](#)]
55. Schmidt, T.; Schuster, C.; Kleinschmit, B.; Forster, M. Evaluating an Intra-Annual Time Series for Grassland Classification - How Many Acquisitions and What Seasonal Origin Are Optimal? *IEEE J. Sel. Top. Appl. Earth Obs. Remote Sens.* **2014**, *7*, 3428–3439. [[CrossRef](#)]
56. Vuolo, F.; Richter, K.; Atzberger, C. Evaluation of time-series and phenological indicators for land cover classification based on MODIS data. In *Proceedings of SPIE 8174, Remote Sensing for Agriculture, Ecosystems, and Hydrology XIII*; Neale, C.M.U., Maltese, A., Eds.; Prague, Czech Republic, 19 September 2011.
57. Waldner, F.; Lambert, M.-J.; Li, W.; Weiss, M.; Demarez, V.; Morin, D.; Marais-Sicre, C.; Hagolle, O.; Baret, F.; Defourny, P. Land Cover and Crop Type Classification along the Season Based on Biophysical Variables Retrieved from Multi-Sensor High-Resolution Time Series. *Remote Sens.* **2015**, *7*, 10400–10424. [[CrossRef](#)]
58. Duro, D.C.; Franklin, S.E.; Dubé, M.G. A comparison of pixel-based and object-based image analysis with selected machine learning algorithms for the classification of agricultural landscapes using SPOT-5 HRG imagery. *Remote Sens. Environ.* **2012**, *118*, 259–272. [[CrossRef](#)]
59. Waser, L.T.; Küchler, M.; Jütte, K.; Stampfer, T. Evaluating the Potential of WorldView-2 Data to Classify Tree Species and Different Levels of Ash Mortality. *Remote Sens.* **2014**, *6*, 4515–4545. [[CrossRef](#)]
60. Feilhauer, H.; Dahlke, C.; Doktor, D.; Lausch, A.; Schmidtlein, S.; Schulz, G.; Stenzel, S. Mapping the local variability of Natura 2000 habitats with remote sensing. *Appl. Veg. Sci.* **2014**, *17*, 765–779. [[CrossRef](#)]
61. Radoux, J.; Bogaert, P. Accounting for the area of polygon sampling units for the prediction of primary accuracy assessment indices. *Remote Sens. Environ.* **2014**, *142*, 9–19. [[CrossRef](#)]
62. Ozdemir, I. Linear transformation to minimize the effects of variability in understory to estimate percent tree canopy cover using RapidEye data. *GIScience Remote Sens.* **2014**, *51*, 288–300. [[CrossRef](#)]
63. Schlerf, M.; Atzberger, C.; Hill, J. Tree Species and Age Class Mapping in a Central European Woodland Using Optical Remote Sensing Imagery and Orthophoto Derived Stem Density—Performance of Multispectral and Hyperspectral Sensors. In *Geoinformation for European-wide integration. Proceedings of the 22nd Symposium of the European Association of Remote Sensing Laboratories, Prague, Czech Republic, 4–6 June 2002; 2003*; pp. 413–418.
64. Clark, M.L.; Roberts, D.A.; Clark, D.B. Hyperspectral discrimination of tropical rain forest tree species at leaf to crown scales. *Remote Sens. Environ.* **2005**, *96*, 375–398. [[CrossRef](#)]

65. Leckie, D.G.; Tinis, S.; Nelson, T.; Burnett, C.; Gougeon, F.A.; Cloney, E.; Paradine, D. Issues in species classification of trees in old growth conifer stands. *Can. J. Remote Sens.* **2005**, *31*, 175–190. [[CrossRef](#)]
66. Carleer, A.; Wolff, E. Exploitation of very high resolution satellite data for tree species identification. *Photogramm. Eng. Remote Sens.* **2004**, *70*, 135–140. [[CrossRef](#)]
67. Immitzer, M.; Atzberger, C.; Koukal, T. Eignung von WorldView-2 Satellitenbildern für die Baumartenklassifizierung unter besonderer Berücksichtigung der vier neuen Spektralkanäle. *Photogramm. Fernerkund. Geoinformation.* **2012**, *5*, 573–588. [[CrossRef](#)]
68. Kim, S.-R.; Lee, W.-K.; Kwak, D.-A.; Biging, G.S.; Gong, P.; Lee, J.-H.; Cho, H.-K. Forest cover classification by optimal segmentation of high resolution satellite imagery. *Sensors* **2011**, *11*, 1943–1958. [[CrossRef](#)] [[PubMed](#)]
69. Immitzer, M.; Toscani, P.; Atzberger, C. The Utility of Wavelet-based Texture Measures to Improve Object-based Classification of Aerial Images. *South.-East. Eur. J. Earth Obs. Geomat.* **2014**, *3*, 79–84.
70. Liu, X.; Bo, Y. Object-Based Crop Species Classification Based on the Combination of Airborne Hyperspectral Images and LiDAR Data. *Remote Sens.* **2015**, *7*, 922–950. [[CrossRef](#)]
71. Ramoelo, A.; Cho, M.; Mathieu, R.; Skidmore, A.K. Potential of Sentinel-2 spectral configuration to assess rangeland quality. *J. Appl. Remote Sens.* **2015**, *9*. [[CrossRef](#)]
72. Schuster, C.; Förster, M.; Kleinschmit, B. Testing the red edge channel for improving land-use classifications based on high-resolution multi-spectral satellite data. *Int. J. Remote Sens.* **2012**, *33*, 5583–5599. [[CrossRef](#)]
73. Elatawneh, A.; Rappl, A.; Rehush, N.; Schneider, T.; Knoke, T. Forest tree species identification using phenological stages and RapidEye data: A case study in the forest of Freising. In Proceedings of the 5th RESA Workshop, Neustrelitz, Germany, 20–21 March 2013; pp. 21–38.
74. Li, D.; Ke, Y.; Gong, H.; Li, X. Object-Based Urban Tree Species Classification Using Bi-Temporal WorldView-2 and WorldView-3 Images. *Remote Sens.* **2015**, *7*, 16917–16937. [[CrossRef](#)]
75. Tigges, J.; Lakes, T.; Hostert, P. Urban vegetation classification: Benefits of multitemporal RapidEye satellite data. *Remote Sens. Environ.* **2013**, *136*, 66–75. [[CrossRef](#)]
76. Wulder, M.A.; Hilker, T.; White, J.C.; Coops, N.C.; Masek, J.G.; Pflugmacher, D.; Crevier, Y. Virtual constellations for global terrestrial monitoring. *Remote Sens. Environ.* **2015**, *170*, 62–76. [[CrossRef](#)]



© 2016 by the authors; licensee MDPI, Basel, Switzerland. This article is an open access article distributed under the terms and conditions of the Creative Commons by Attribution (CC-BY) license (<http://creativecommons.org/licenses/by/4.0/>).